

Exciton optical absorption in asymmetric ZnO/ZnMgO double quantum wells with mixed phases

Zhi-Qiang Han(韩智强), Li-Ying Song(宋丽颖), Yu-Hai Zan(昝宇海), Shi-Liang Ban(班士良)

Citation: Chin. Phys. B . 2020, 29(7): 077104 . **doi:** 10.1088/1674-1056/ab8d9d
Journal homepage: http://cpb.iphy.ac.cn; http://iopscience.iop.org/cpb

What follows is a list of articles you may be interested in

Visualizing light-to-electricity conversion process in InGaN/GaN multi-quantum wells with a p-n junction

Yangfeng Li(李阳锋), Yang Jiang(江洋), Junhui Die(迭俊珲), Caiwei Wang(王彩玮), Shen Yan(严珅), Haiyan Wu(吴海燕), Ziguang Ma(马紫光), Lu Wang(王禄), Haiqiang Jia(贾海强), Wenxin Wang(王文新), Hong Chen(陈弘)

Chin. Phys. B . 2018, 27(9): 097104 . **doi:** 10.1088/1674-1056/27/9/097104

Intersubband optical absorption of electrons in double parabolic quantum wells of $Al_xGa_{1-x}As/Al_yGa_{1-y}As$

Shu-Fang Ma(马淑芳), Yuan Qu(屈媛), Shi-Liang Ban(班士良)

Chin. Phys. B . 2018, 27(2): 027103 . **doi:** 10.1088/1674-1056/27/2/027103

Effects of electron-optical phonon interactions on the polaron energy in a wurtzite $ZnO/M_xZn_{1-x}O$ quantum well

Zhao Feng-Qi, Zhang Min, Bai Jin-Hua

Chin. Phys. B . 2015, 24(9): 097105 . **doi:** 10.1088/1674-1056/24/9/097105

Spatially nonlocal effects on optical absorption properties incoupled quantum wells with an applied electric field

Wang Chao-Yang, Wang Guang-Hui

Chin. Phys. B . 2014, 23(12): 127103 . **doi:** 10.1088/1674-1056/23/12/127103

A theoretical investigation of the band alignment of type-I direct band gap dilute nitride phosphide alloy of $GaN_xAs_yP_{1-x-y}$/GaP quantum wells on GaP substrates

Ö L Ünsal, B Gönül, M Temiz

Chin. Phys. B . 2014, 23(7): 077104 . **doi:** 10.1088/1674-1056/23/7/077104

Exciton optical absorption in asymmetric ZnO/ZnMgO double quantum wells with mixed phases*

Zhi-Qiang Han(韩智强), Li-Ying Song(宋丽颖), Yu-Hai Zan(昝宇海), and Shi-Liang Ban(班士良)†

School of Physical Science and Technology, Inner Mongolia University, Hohhot 010021, *China*

(Received 21 December 2019; revised manuscript received 18 April 2020; accepted manuscript online 28 April 2020)

The optical absorption of exciton interstate transition in $Zn_{1-xl}Mg_{xl}O/ZnO/Zn_{1-xc}Mg_{xc}O/ZnO/Zn_{1-xr}Mg_{xr}O$ asymmetric double quantum wells (ADQWs) with mixed phases of zinc-blende and wurtzite in $Zn_{1-x}Mg_xO$ for $0.37 < x < 0.62$ is discussed. The mixed phases are taken into account by our weight model of fitting. The states of excitons are obtained by a finite difference method and a variational procedure in consideration of built-in electric fields (BEFs) and the Hartree potential. The optical absorption coefficients (OACs) of exciton interstate transition are obtained by the density matrix method. The results show that Hartree potential bends the conduction and valence bands, whereas a BEF tilts the bands and the combined effect enforces electrons and holes to approach the opposite interfaces to decrease the Coulomb interaction effects between electrons and holes. Furthermore, the OACs indicate a transformation between direct and indirect excitons in zinc-blende ADQWs due to the quantum confinement effects. There are two kinds of peaks corresponding to wurtzite and zinc-blende structures respectively, and the OACs merge together under some special conditions. The computed result of exciton interband emission energy agrees well with a previous experiment. Our conclusions are helpful for further relative theoretical studies, experiments, and design of devices consisting of these quantum well structures.

Keywords: quantum well, mixed phase, exciton transition, direct and indirect exciton, optical absorption

PACS: 71.35.–y, 78.20.Ci, 73.21.Fg, 71.55.Gs **DOI:** 10.1088/1674-1056/ab8d9d

1. Introduction

Double quantum wells (DQWs) have attracted attention due to their potential applications in low threshold lasers,[1,2] photoswitches,[3] and phase modulators[4] since last two decades. Compared with symmetric DQWs, the carrier levels and distribution in asymmetric double quantum wells (ADQWs)[3] are more complex due to the asymmetric quantum confinement. As a ZnO involved wide gap semiconductors, the excitons and their related polaritons became observable at room temperature.[5,6] It is worthy to discuss the exciton related phenomena in ADQWs since they are the basic structures of devices.

It was well known that the stable structure of ZnO is wurtzite one, within the incorporation of Mg the structure of ternary mixed crystals (TMCs) $Zn_xMg_{1-x}O$ will change from a single wurtzite one to a mixed phase with both of wurtzite and zinc-blende in the range of $0.37 < x < 0.62$.[7] For zinc-blende, only piezoelectric polarization (PP) contributes to built-in electric fields (BEFs), whereas the BEFs are formed by both of the PP and spontaneous polarization (SP) for wurtzite.[8,9] On the other hand, the physical parameters such as carrier effective masses, elastic and piezoelectric constants and band gaps, *etc*. are also different for the two kinds of structures. Thus, the exciton states show an obvious difference due to a sharp distinction of these parameters between wurtzite and zinc-blende. As a result, there are different transitions in wurtzite and zinc-blende structures respectively between the same exciton energy levels and the OACs should be studied necessarily in mixed phases.[10–13]

In 2010, Zippel *et al.*[14] fabricated $ZnO/Zn_{1-x}Mg_xO$ single QWs to show experimentally the modulations of the size and Mg components for exciton transitions. A clear blue shift of the photoluminescence peak with decreasing well width was observed. Additionally, the exciton transition energy increases with increasing x, whereas the authors just considered a single wurtzite of $Zn_xMg_{1-x}O$. Later, Segawa*et al.*[15] manufactured ten periods of ZnO/ZnMgO multiple QWs by pulsed laser deposition, and measured the optical absorption spectra to give the absorption peaks of exciton transitions. However, the explicit exciton states corresponding to the absorption peaks were neglected, and even without discussion of the modulation of exciton optical absorption by Mg components. More recently, Stachowiczet *et al.*[16] demonstrated $ZnO/Zn_{1-x}Mg_xO$ ADQWs of high quality by molecular beam epitaxy technique, and the photoluminescence spectra of excitons with different components were obtained. The coupling between the wells by tunneling of charge carries from a narrow well to the wider well was found. In 2011, Yu *et al.*[17] investigated theoretically the OACs of ZnO/ZnMgO quantum wells by the fractional-dimensional space approach with consideration of exciton effects, and indicated that the peaks move to a lower energy. In 2017, Gu *et al.*[18] calculated the OACs of electron interband transitions in wurtzite ZnO/ZnMgO quantum wells in consideration of built-in electric fields (BEFs) and the Hartree potential, and the effects of size and TMCs of OACs are also given. Recently, Song *et al.*[19] investigated optical absorption of exciton transitions in a single QW by introducing a mixed phase model.

*Project supported by the National Natural Science Foundation of China (Grant No. 61764012).

†Corresponding author. E-mail: slban@imu.edu.cn

© 2020 Chinese Physical Society and IOP Publishing Ltd

In the present research, a finite difference method and a variational procedure were used to compute the exciton states in $Zn_{1-xl}Mg_{xl}O/ZnO/Zn_{1-xc}Mg_{xc}O/ZnO/Zn_{1-xr}Mg_{xr}O$ ADQWs, within a wider x range by considering the influence of BEFs and the Hartree potential. Compared with the existing theoretical works, this method can obtain energy levels of excitronic subband more efficiently. The OACs of exciton interstate transition in ADQWs are calculated by the density matrix method. In this process, we use the weight model to discuss the influence of $Zn_xMg_{1-x}O$ ($0.37 < x < 0.62$) mixed phases on the OACs, which was neglected by other authors. The size and TMCs effects of OACs were investigated in the case of the whole composition. Up to now, there are few experimental reports about the OACs of exciton interstates transition in ADQWs with mixed phases, so the exciton interband emission is calculated for a simple structure. The part of our results is compared with the experiment to verify the feasibility of this method. The paper is organized as follows: the theory and model used in our works are described in Section 2. Section 3 gives the computed results and discussions. Finally, the conclusions are shown in Section 4.

2. Theory and model

Let us assume that an exciton is confined in a $Zn_{1-xl}Mg_{xl}O/ZnO/Zn_{1-xc}Mg_{xc}O/ZnO/Zn_{1-xr}Mg_{xr}O$ ADQW as shown in Fig. 1. Here, L_{b1}, L_b, and L_{b2} are chosen as the thicknesses corresponding to the left, center, and right barriers. L_{w1} and L_{w2} are the wideness of left and right wells of the ADQWs, respectively. The growth direction of materials is chosen as the z axis whereas the perpendicular to this direction as the x–y plane. The Hamiltonian of the exciton in this ADQW can be expressed by

$$H = H_{e-h} + H(z_e) + H(z_h). \tag{1}$$

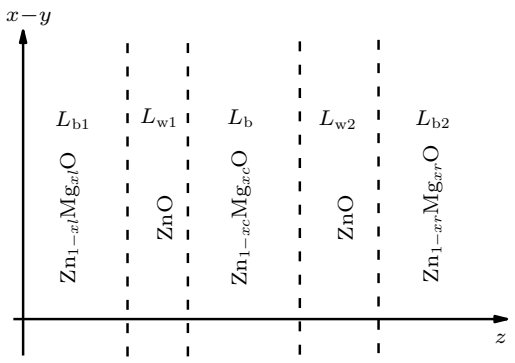


Fig. 1. The schematic diagram of a $Zn_{1-xl}Mg_{xl}O/ZnO/Zn_{1-xc}Mg_{xc}O/ZnO/Zn_{1-xr}Mg_{xr}O$ ADQW.

In Eq. (1), H_{e-h} consists of two parts, the kinetic energy term of the electron–hole in the x–y plane and the Coulomb interaction between the electron and hole with charge e and $-e$, respectively.[20,21] It can be given by

$$H_{e-h} = -\frac{\hbar^2}{2\mu(z_e,z_h)}\frac{1}{\rho}\frac{\partial}{\partial\rho}\rho\frac{\partial}{\partial\rho} - \frac{e^2}{4\pi\varepsilon_0\varepsilon(z_e,z_h)\sqrt{\rho^2+(z_e-z_h)^2}}. \tag{2}$$

In Eq. (2), $\hbar = h/2\pi$, where h is the Planck constant. $\mu(z_e,z_h) = m_e^{\parallel}(z_e)m_h^{\parallel}(z_h)/(m_e^{\parallel}(z_e)+m_h^{\parallel}(z_h))$ is the reduced mass of an electron–hole pair with their z-dependent masses $m_e^{\parallel}(z_e)$ and $m_h^{\parallel}(z_h)$ in the x–y plane, respectively.

$$\rho = \sqrt{(x_e-x_h)^2+(y_e-y_h)^2}$$

represents the distance between the electron and hole in the x–y plane. ε_0 is the static dielectric constant of vacuum. $\varepsilon(z_e,z_h)$ is the relative dielectric constant that is related to the position of the electron and hole.

In Eq. (1), $H(z_i)$ (i = e, h) are the parts of Hamiltonian for a single electron and hole in the z direction. They can be written as

$$H(z_i) = -\frac{\hbar^2}{2}\frac{\partial}{\partial z}\left[\frac{1}{m_i^*(z)}\right]\frac{\partial}{\partial z} + V_i + V_{H,i} + qF_kz, \tag{3}$$

In Eq. (3), $m_i^*(z)$ are the z-dependent effective masses of the electron and hole in the z direction, respectively. q is the charge e ($-e$) of the electron (hole). V_i are the confinement potential for the electron and hole in the z direction, and can be expressed as following according to the rule of 7 : 3[18]

$$V_i = R\times\left(E_{g,ZnMgO} - E_{g,ZnO}\right), \tag{4}$$

where $R = 0.7$ for i = e and $R = 0.3$ for i = h.

Here $E_{g,ZnMgO}$ is the band gap of $Zn_{1-x}Mg_xO$ and can be given by $E_{g,ZnMgO} = xE_{g,MgO} - (1-x)E_{g,ZnO}$, where xr epresents the component of Mg. $E_{g,MgO}$ and $E_{g,ZnO}$ are the band gaps for MgO and ZnO alloys, respectively.

In Eq. (3), $V_{H,i}$ is the Hartree potential induced by the distribution of free carriers, it satisfies Poisson equation[22] for electron and hole

$$\frac{d}{dz}\left[\varepsilon_0\varepsilon_k\frac{d}{dz}V_{H,i}(z)\right] = -e^2\left[N_{D,i}^+ - N_{2D}(z_i)\right], \quad (k = b1, w1, b, w2, b2), \tag{5}$$

where ε_k is the relative dielectric constant of the k-th layer material, N_D^+ the ionized donor concentration and $N_{2D}(z_i)$ the two-dimensional electron (hole) gas density. N_D^+ satisfies

$$N_{D,i}^+ = N_D\left(\frac{1}{1+2\exp\left[(E_{f,i}-E_D)/k_BT\right]}\right). \tag{6}$$

N_D is the doping concentration at temperature T.[18] $E_{f,i}$ is the Fermi energy and E_D the donor energy level. And k_B is the Boltzmann constant. In Eq. (5), $N_{2D}(z_i)$ is the two-dimensional electron (hole) gas concentration in all conduction (valance) sub-band related to the distribution of electron (hole). And it satisfies[23]

$$N_{2D}(z_i) = \sum_n \frac{m_i^*(z)k_BT}{\pi\hbar^2}|\varphi_n(z_i)|^2 \times\ln\left[1+\exp\left(\frac{E_{f,i}-E_{n,i}}{k_BT}\right)\right] \quad (n = 1,2,3,\ldots), \tag{7}$$

where $\varphi_n(z_i)$, $E_{n,i}$ is the electron (hole) wave function and energy corresponding to the n-th energy level in the z direction. In Eq. (7), $E_{f,i}$ can be given by self-consistently solving the condition of electric neutrality for electrons and holes in the total thickness $L = L_{b1} + L_{w1} + L_b + L_{w2} + L_{b2}$ of the ADQW as follows:[24]

$$\int_0^L \left[N_{D,i}^+ - N_{2D}(z_i) \right] \mathrm{d}z = 0. \tag{8}$$

It should be noted that the Hartree potential at the boundary is 0 in Eq. (5), that is $V_{H,i}(0) = 0$, and $V_{H,i}(L) = 0$.

In Eq. (3), F_k is the BEF in layer k, and it can be expressed as follows:[25]

$$F_k = \frac{\sum_l L_l (P_l^{tot} - P_k^{tot})/\varepsilon_0 \varepsilon_l}{\varepsilon_k \sum_l L_l/\varepsilon_l}, \quad k,l = b1, w1, b, w2, b2, \tag{9}$$

where L_l represents the thickness of layer l in the ADQW. For a wurtzite structure, the total polarization P_k^{tot} was described in detail in Ref. [18]

For a zinc-blende structure, P_k^{tot} is just induced by the P_k^{pp} and can be written as[26]

$$P_k^{tot} = P_k^{pp} = 2e_{14,k} \times \kappa_{zz,k}, \tag{10}$$

where

$$\kappa_{zz,k} = \kappa_{xx,k} \frac{(2C_{11,k} + 2C_{12,k} - 4C_{44,k})}{(C_{11,k} + 2C_{12,k} + 4C_{44,k})}, \quad \kappa_{xx,k} = \frac{(a_{MgO} - a_{ZnMgO})}{a_{ZnMgO}}. \tag{11}$$

In Eq. (10), $e_{14,k}$ is the piezoelectric coefficient. In Eq. (11), a_{MgO} and a_{ZnMgO} are the lattice constants of bulk materials MgO and ZnMgO, respectively. $C_{11,k}$, $C_{12,k}$, and $C_{44,k}$ are elasticity constants for a zinc-blend. The lattice constant of a TMC can be interpolated linearly by binary compounds and satisfies $a_{ZnMgO} = x a_{MgO} + (1-x) a_{ZnO}$.[16]

Let us consider that exciton transition is only caused by the transition of the electron (hole) in the z direction mainly due to the confinement potential since the separation between the ground state and first excited state caused by Coulomb interaction is larger than the photon energy within infrared region, and the exciton is at the ground state in the x–y plane. So that its excited states can be written as[27]

$$\psi_j(\lambda) = D\varphi_n(z_e)\,\varphi_m(z_h)\,\varphi(\rho, z_e, z_h, \lambda), \tag{12}$$

where D is the normalized coefficient. Here, $\varphi_n(z_e)$ and $\varphi_m(z_h)$ are the eigenstates for a single electron and hole, respectively. They can be obtained by self-consistently solving the Schrödinger equation

$$H(z_i)|\varphi_{n(m)}(z_i)\rangle = E_{n(m)}|\varphi_{n(m)}(z_i)\rangle, \tag{13}$$

and Poisson equation (5). In Eq. (12), trial wave function

$$\varphi(\rho, z_e, z_h, \lambda) = \exp\left(-\lambda\sqrt{\rho^2 + (z_e - z_h)^2}\right),$$

where λ is a variational parameter and can be determined by the following procedure of minimizing the ground state energy[26]

$$E_{min} = \frac{\partial \langle D\varphi_1(z_e)\,\varphi_1(z_h)\,\varphi(\rho, z_e, z_h, \lambda)|H|D\varphi_1(z_e)\,\varphi_1(z_h)\,\varphi(\rho, z_e, z_h, \lambda)\rangle}{\partial\lambda}. \tag{14}$$

The excited state energies of excitons can be expressed as

$$E_j = \langle D\varphi_n(z_e)\,\varphi_m(z_h)\,\varphi(\rho, z_e, z_h, \lambda)| \times H|D\varphi_n(z_e)\,\varphi_m(z_h)\,\varphi(\rho, z_e, z_h, \lambda)\rangle. \tag{15}$$

Here, m and n are not equal to 1 simultaneously.

The OACs of exciton transitions can be written as[28]

$$\alpha_{jj'}(\omega) = \omega\sqrt{\frac{\mu}{\varepsilon_0}} \frac{|M_{jj'}|^2 \sigma_s \hbar\Gamma_{jj'}}{\hbar^2(\omega - \omega_{jj'})^2 + (\hbar\Gamma_{jj'})^2}, \tag{16}$$

where ω is the frequency of an incident photon, μ the permeability of vacuum. Dipole matrix element $M_{jj'}$ can be written as the following expression[29]

$$M'_{jj} = \langle \psi_j | q(z_e - z_h) | \psi_{j'} \rangle. \tag{17}$$

In Eq. (16), $\omega_{jj'} = \Delta E/\hbar$. Here, ΔE is the exciton interstate transition energy, σ_s the electron density in the well. Γ_{mn} is the relaxation rate.

There are two phases of zinc-blende and wurtzite in $Zn_{1-x}Mg_xO$ for $0.37 < x < 0.62$.[10] We assume that the mixed phase can be fitted with a Gauss pacific distribution and the proportion of zinc-blende in the structure can be expressed as follows:[19]

$$G(x) = \frac{1}{\sqrt{2\pi}\delta} \int_0^x \exp\left[-\frac{(y-\eta)^2}{2\delta^2}\right] \mathrm{d}y. \tag{18}$$

It was named as the weight model with expected value η and variance δ. η and δ are given in Section 3. The OACs in the mixed phase can be interpolated by

$$\alpha_{jj'}^{mix}(\omega) = \alpha_{jj'}^{ZB}(\omega) \times G(x) + \alpha_{jj'}^{WZ}(\omega) \times (1 - G(x)), \tag{19}$$

where $\alpha_{jj'}^{ZB}$ and $\alpha_{jj'}^{WZ}$ are the optical absorption coefficients in the $Zn_{1-xl}Mg_{xl}O/ZnO/Zn_{1-xc}Mg_{xc}O/ZnO/Zn_{1-xr}Mg_{xr}O$ ADQW of which the barriers are zinc-blende and wurtzite, whereas the wells are wurtzite for both cases of barriers. The former is named ADQW1 and the latter is named ADQW2 in the following.

3. Results and discussion

The parameters used in the numerical calculation are given in Table 1. In addition, in Eq. (6) $N_D = 5 \times 10^{19}/\text{cm}^3$. In Eq. (7), E_D is adopted as 0.03 eV below the bottom of the conduction band. We choose $\eta = 0.5$ and $\delta = 0.25$ in Eq. (18), and $\Gamma_{mn} = 0.14$ ps.[14]

In order to show the influence of Hartree potential $V_{H,i}$ on the total potentials, the potential profiles before and after the self-consistent computations and $V_{H,i}$ are given for specified ADQW1 with well widths of $L_{w1} = 6$ nm and $L_{w2} = 4$ nm and the width of central barrier with $L_b = 1.5$ nm in Fig. 2.

Table 1. Material parameters about ZnO and MgO of WZ and ZB used in the calculations.

		Wurtzite			Zinc-blende	
		ZnO	MgO		ZnO	MgO
Lattice constant/nm	a[a]	0.3219	0.3259	a[b]	0.4538	0.4436
Elasticity constants/GPa	C_{11}[a]	217	222	C_{11}[b]	193	159
	C_{12}[a]	117	90	C_{12}[b]	139	133.3
	C_{13}[a]	121	58	C_{44}[b]	96	74
	C_{33}[a]	225	109			
Piezoelectric coefficients/(c/m^2)	e_{31}[a]	–0.57	–0.38	e_{14}[b]	0.69	0.78
	e_{33}[a]	1.34	2.26			
Spontaneous polarization[a]/(c/m^2)	P^{sp}	–0.022	–0.06			
Bad gap/eV	E_g	3.37[c]	6.34[d]	E_g	3.27[e]	7.8[f]
Effective mass (free electron mass m_0)	m_e^*	0.24[g]	0.35[f]	m_e^*	0.233[h]	0.24[i]
	m_h^*	0.78[j]	1.6[f]	m_h^*	1.578[h]	0.78[i]

[a]Ref. [30]; [b]Ref. [31]; [c]Ref. [32]; [d]Ref. [33]; [e]Ref. [34]; [f]Ref. [35]; [g]Ref. [36]; [h]Ref. [19]; [i]Ref. [26]; [j]Ref. [37].

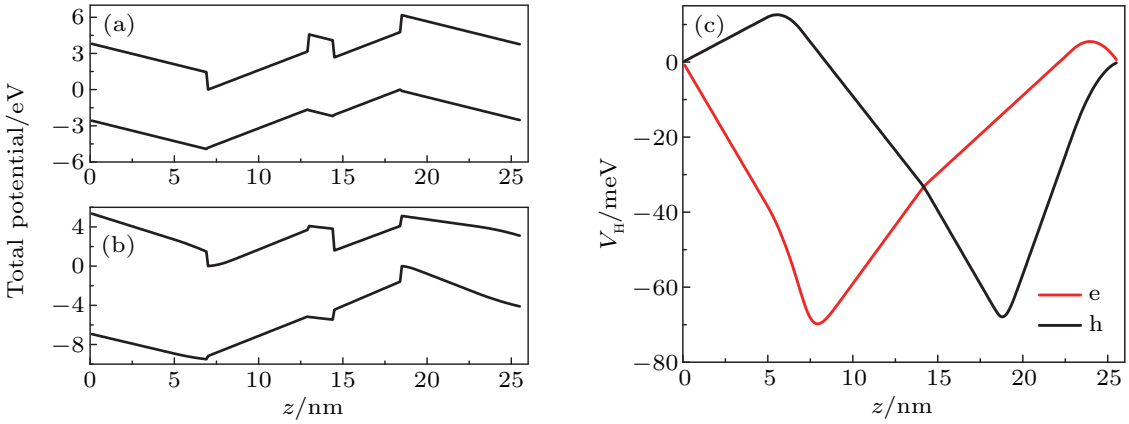


Fig. 2. Total potential profiles before (a), after (b) self-consistent computations, and Hartree potential $V_{H,i}$ (c) for electrons (holes) in the specified ADQW1.

It can be seen from Figs. 2(a) and 2(b) that $V_{H,i}$ bends the conduction and valance bands to lower (elevate) the energy levels of electrons (holes). Consequently, this effect strengths the binding of excitons. Figure 2(c) also indicates boundary condition for Eq. (5).

The eigen-wavefunctions and corresponding energy levels of the electron (hole) are computed for ADQW2 and ADQW1 mentioned in Section 2 by solving Eqs. (5) and (13) with parameters in Table 1. According to Eq. (15), the three energy levels of an exciton are calculated to be $E_1(e_1h_1)$, $E_2(e_1h_3)$, and $E_3(e_2h_1)$, where e_i (h_i) presents an electron (hole) at state i. The OACs of exciton transitions between these energy levels are calculated based on the density matrix principle and the OACs for mixed phases and are obtained by the weight model interpolated by Eq. (19). In order to verify the feasibility of our theory, the exciton interband emission energy in ADQW2 is denoted by $E_{ph} = E_e + E_h + E_g - E_b$ with E_e and E_h as the confinement energies of the electron and hole respectively, E_g as the band gap energy of ZnO, and E_b as the exciton binding energy. Our computed result agrees well with the experiment[38] for a special asymmetric structure with equal height of wells and barriers and the corresponding OACs are presented in Fig. 3.

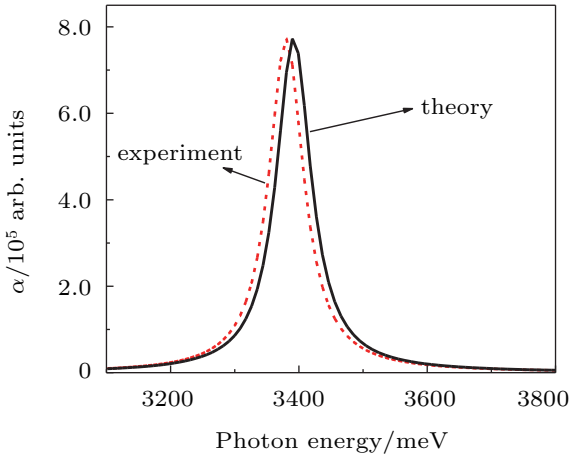


Fig. 3. The OACs of the exciton interband transition as a function of the incident photon energy in a $Zn_{0.85}Mg_{0.15}O/ZnO/Zn_{0.85}Mg_{0.15}O/ZnO/Zn_{0.85}Mg_{0.15}O$ (9 nm/2 nm/2 nm/7 nm/9 nm) ADQW. The red dash line is the experimental result.[38] and the black solid line represents our theoretical result.

Figure 4 shows the optical absorption coefficients for the exciton transition of E_1 to E_3 with variation of L_b in the two kinds of ADQWs. The two kinds of peaks are given in Figs. 4(a) and 4(b) to present the results for ADQW1 and the ADQW2, respectively. For the two cases, the hole is in the right well, whereas the electron can stay in the two wells to form a direct exciton or an indirect exciton. It can be seen from Fig. 4, the variation of the optical absorption coefficients is insensitive to the variation of L_b for $L_{w1} = L_{w2}$ in ADQW2 that indicates the exciton is direct. Whereas an obvious red shift appears in Fig. 4(a) when L_b increases from 1.7 nm for ADQW1. This phenomenon is due to the change of the excitons from the indirect type to the direct type. For a direct exciton, the electron is mainly distributed in the right well with a lower barrier potential because of the quantum confinement effects (QCEs). The formation of indirect excitons is that the electron tunnels into the left well within the influence of the BEFs when $L_b < 1.7$ nm, whereas the hole remains in the right well with the increase of L_b. It should be pointed out that the BEF has a stronger influence on the indirect exciton to separate the electron and hole. During the transition, the electron plays an important role. The energy level intervals of the electron in the left well with a higher barrier potential are larger than that in the right well with a lower barrier potential. Consequently the change of the exciton type results in a redshift of the optical absorption coefficients. When $L_{w1} > L_{w2}$, the tunneling of the electron in the right well into the left well is easier under the strong quantum confinement effects as decreasing L_b to keep the exciton being indirect. As a result, it can be seen that the optical absorption coefficients only have a slightly red shift caused by the weakened BEFs in the left well with decreasing L_b for ADQW1 in Fig. 4(b).

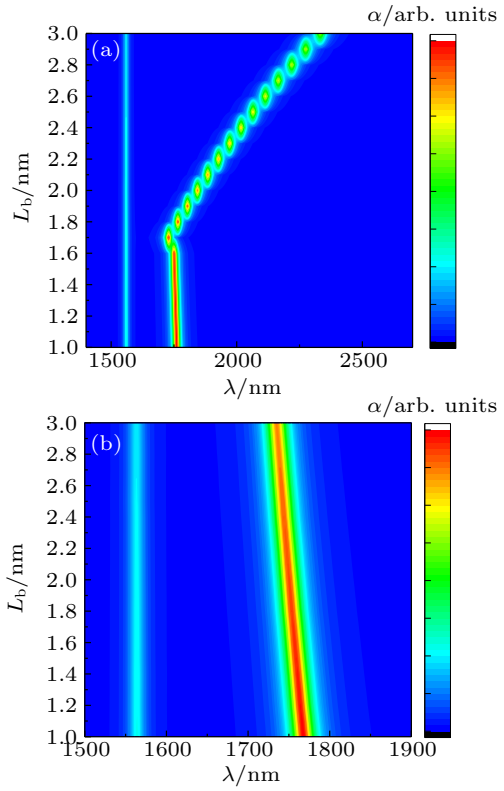


Fig. 4. OACs of the exciton transition from E_1 to E_3 with variation of incident photon wavelength λ as a function of L_b for $Zn_{1-xl}Mg_{xl}O/ZnO/Zn_{1-xc}Mg_{xc}O/ZnO/Zn_{1-xr}Mg_{xr}O$ ADQWs with $L_{b1} = 7$ nm, $L_{b2} = 7$ nm, $xl = 0.6$, $xc = 0.4$, and $xr = 0.4$ for (a) $L_{w1} = 4$ nm and $L_{w2} = 4$ nm; (b) $L_{w1} = 5$ nm and $L_{w2} = 3$ nm. The right images are for ADQW1, the left ones for ADQW2.

Figure 5 shows the OACs of the exciton transition from E_2 to E_3 with variation of L_b when $L_{w1} = L_{w2}$ and $L_{w1} > L_{w2}$ for ADQW1 and ADQW2, respectively. As discussed for Fig. 4, it can be clearly seen that there is a transition between a direct and an indirect excitons near $L_b \sim 1.7$ nm for ADQW1. The BEF in the central barrier is weakened gradually as increase of L_b, and the BEFs in the wells also increase. There three effects enhance the QCEs on the electron and hole in different wells to increase the intervals of exciton energy levels for ADQW2. As a result, both panels 5(a) and 5(b) show that OACs appear a blue shift with increasing L_b. It can be also seen from Fig. 5(a) that the OACs have an obvious blue shift after a red shift for ADQW1 contributed by the exciton-type transformation, which widens the excitonic energy levels intervals due to the stronger Coulomb interaction between electron and hole when $N_b > 1.7$ nm. Figure 5(b) shows that the transition energy decreases gradually as L_b increases in ADQW1 and is contrast to that in ADQW2 when $L_{w1} = L_{w2}$. As increase of L_b for ADQW1 when $L_{w1} > L_{w2}$, the BEFs in the two wells are stronger than that in the central barrier. The BEFs separate the electron and hole to weaken their Coulomb interaction. Consequently, the intervals of excitonic energy levels decrease and the OACs have a red shift. The two kinds of peaks merger together when $L_b = 3$ nm. In addition, the excitonic transition energy from E_1 to E_2 is also calculated. The

result shows that OACs appear a redshift for the two kinds of ADQWs with increasing center barrier thickness. For the sake of shortness, we do not give the results in the paper.

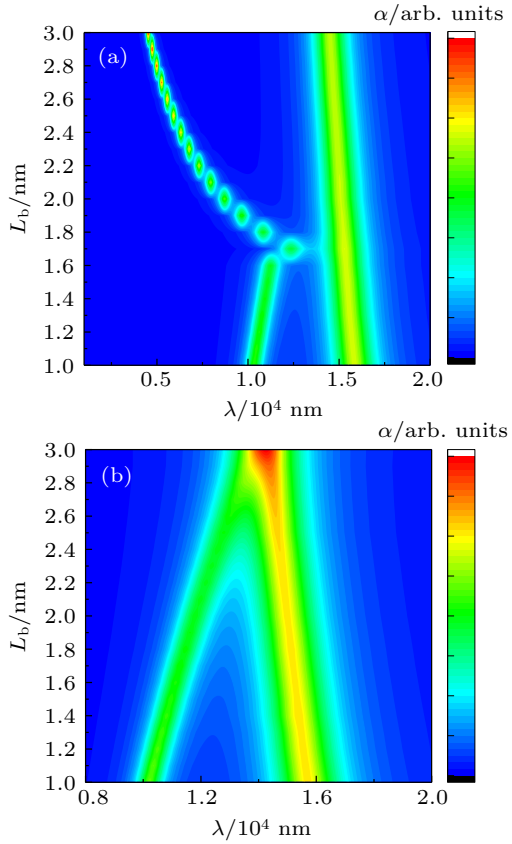


Fig. 5. OACs of the exciton transition from E_2 to E_3 with variation of incident photon wavelength λ as a function of L_b for $Zn_{1-xl}Mg_{xl}O/ZnO/Zn_{1-xc}Mg_{xc}O/ZnO/Zn_{1-xr}Mg_{xr}O$ ADQWs with $L_{b1} = 7$ nm, $L_{b2} = 7$ nm, $xl = 0.6$, $xc = 0.4$, and $xr = 0.4$, for (a) $L_{w1} = 4$ nm and $L_{w2} = 4$ nm; (b) $L_{w1} = 5$ nm and $L_{w2} = 3$ nm. Panel (b) is for ADQW2, panel (a) is for ADQW1.

Figure 6 depicts the wave functions of an electron at e_2 and a hole at h_1 in ADQW1. For comparison, the conduction and valance bands are also given. As shown in Fig. 6(a), it can be seen that the electron and hole are mainly in the right well corresponding to a direct exciton. Whereas the electron and hole are separately in different wells that reveals an indirect exciton. This effect is mainly from the BEFs to tilt the energy bands.

Figure 7 shows the wave functions of direct and indirect excitons at ground state E_1 and excited state E_2 computed using Eq. (12) for both ADQW1 and ADQW2 with the fixed ρ as $\bar{\rho} = \langle \psi_j(\lambda)|\rho|\psi_j(\lambda)\rangle$ (3.16 nm for former and 2.24 nm for later). As shown in Figs. 7(a) and 7(b), the electron and hole distribute mainly in the right well corresponding to a direct exciton at E_1 for ADQW1, whereas the electron and hole are expelled to the opposite directions of the well due to the BEFs and asymmetric properties. It can be seen from Fig. 7(b) that the electron for an exciton at E_2 obviously tunnels into the center barrier and the left well. It can be also seen form Figs. 7(c) and 7(d), the electron and hole distribute in the same wells to form a direct exciton for ADQW2. It can be seen form Figs. 7(c) and 7(d) that the wave functions of exciton at E_1 and E_2 have a wider distribution due to the stronger BEFs. It should be pointed out that the electron in an exciton at E_1 and E_2 has a stronger tunneling effect in ADQW1 comparing with that in ADQW2 since the BEFs are weak for the former. In Figs. 7(e) and 7(f), the electron and hole distribute in the different wells corresponding to an indirect exciton at E_1 and E_2 for ADQW2.

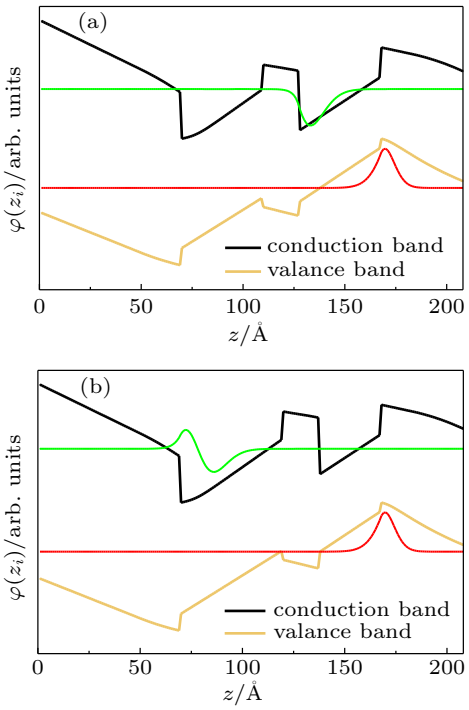


Fig. 6. Wave functions of an electron at e_2 (green lines), a hole at h_1 (red lines) for ADQW1 with $L_{b1} = 7$ nm, $L_{b2} = 4$ nm, $xl = 0.6$, $xc = 0.4$, and $xr = 0.4$ for (a) $L_{w1} = 4$ nm, $L_{w2} = 4$ nm, and (b) $L_{w1} = 5$ nm, $L_{w2} = 3$ nm.

Figure 8 shows the OACs of the exciton transitions from E_1 to E_2, E_2 to E_3, and E_1 to E_3 with increasing L_{w2}, respectively. In Fig. 8(a), the energy level intervals of excitons decrease due to the weakening QCEs. Consequently, the OACs of the transition from E_1 to E_2 have a red shift with increasing L_{w2} for both ADQW1 and ADQW2. Whereas the effect of the Coulomb interaction on the exciton transitions are more important when an energy level of exciton approaches another one. Such like the transition from E_2 to E_3 in Fig. 8(b), the trend of OACs is contrary to that of Fig. 8(a). The differences of average positions between an electron at e_1, e_2, and a hole at h_3, h_1 increase with increasing L_{w2} since the BEFs and asymmetrical structure. The Coulomb interaction becomes weaker to reduce E_2 and E_3, thus the OACs have a blue shift for both of ADQW1 and ADQW2. For the transition from E_1 to E_3 in Fig. 8(c), the intervals of electron energy levels are widened due to the increasing BEF in the left well as increase of L_{w2} to widen interval between E_1 and E_3. As a result, a blue shift appears for both of the ADQWs. At this moment, the electron plays a dominant role in the transition.

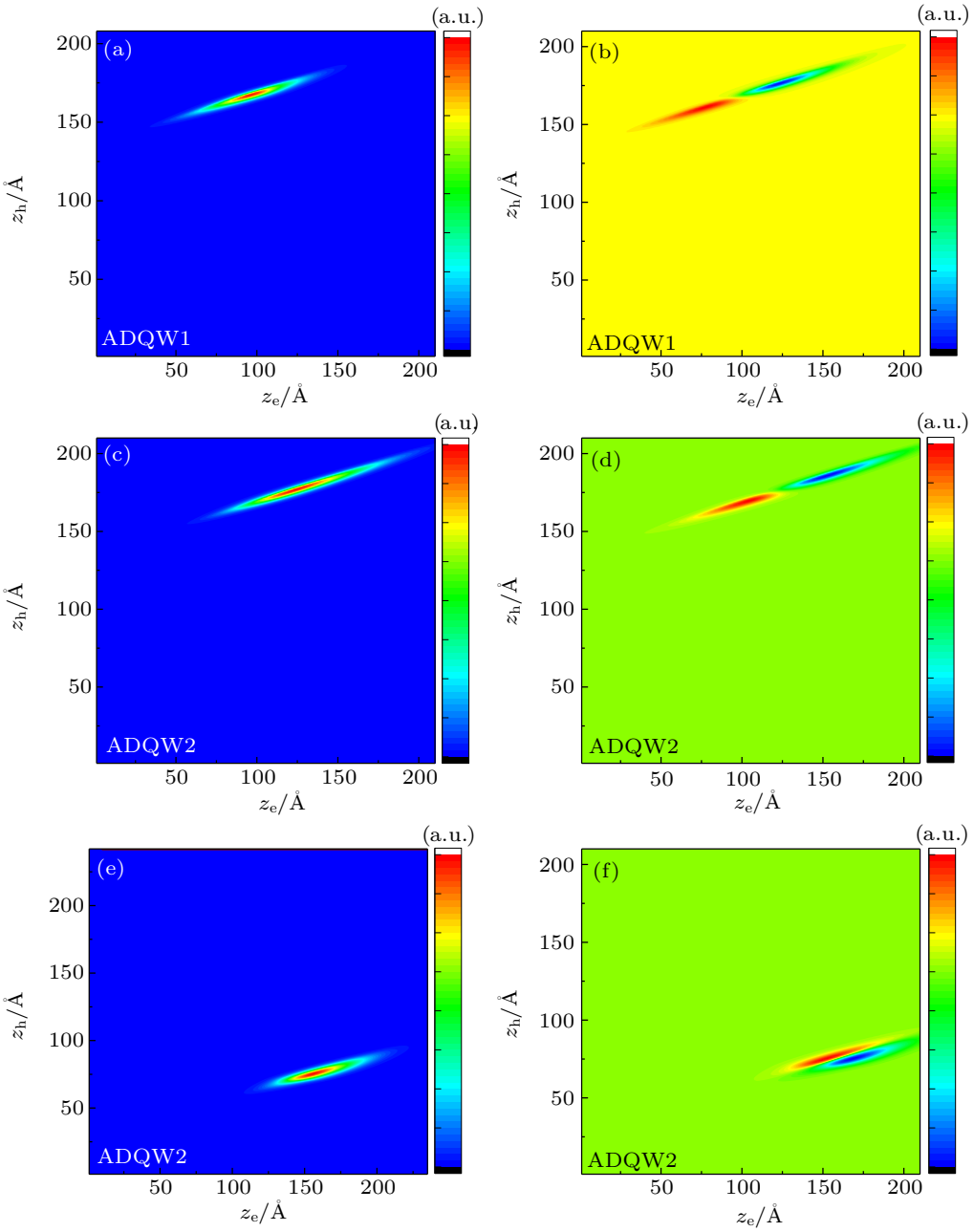


Fig. 7. Wave functions of a direct exciton at state E_1 (a), at state E_2 (b) for ADQW1, at state E_1 (c), and at state E_2 (d) for ADQW2 with $L_{b1} = 7$ nm, $L_{w1} = 5$ nm, $L_b = 1.8$ nm, $L_{w2} = 3$ nm, $L_{b2} = 4$ nm, $xl = 0.6$, $xc = xr = 0.4$, and that of an indirect exciton at state E_1 (e), and at state E_2 (f) for ADQW2 with $L_{b1} = 7$ nm, $L_{w1} = L_{w2} = L_{b2} = 4$ nm, $L_b = 1.8$ nm, $xl = 0.6$, $xc = xr = 0.4$. The unit a.u. is short for arbitrary units.

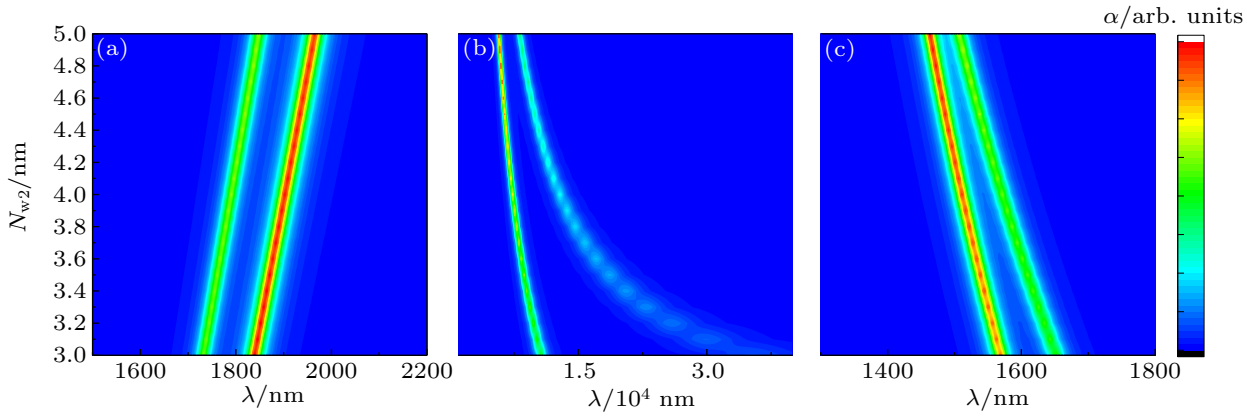


Fig. 8. OACs with the variation of incident photon wavelength λ as a function of L_{w2} for $Zn_{1-xl}Mg_{xl}O/ZnO/ Zn_{1-xc}Mg_{xc}O/ZnO/Zn_{1-xr}Mg_{xr}O$ ADQWs with $L_{b1} = 4$ nm, $L_{w1} = 5$ nm, $L_{b2} = 7$ nm, $xl = 0.6$, $xc = 0.4$, and $xr = 0.4$, for the transition from (a) E_1 to E_2, (b) E_2 to E_3, and (c) E_1 to E_3. The right images are for ADQW1, the left ones are for ADQW2.

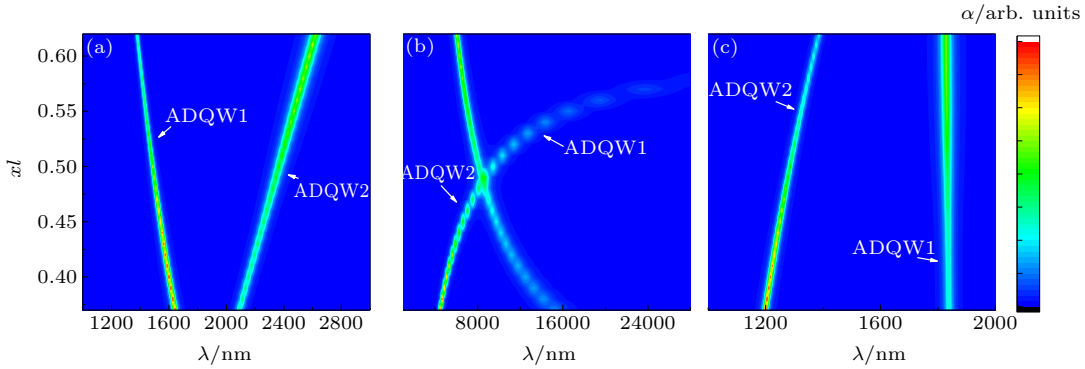


Fig. 9. OACs with the variation of incident photon wavelength λ as a function of xl for $Zn_{1-xl}Mg_{xl}O/ZnO/ Zn_{1-xc}Mg_{xc}O/ZnO/Zn_{1-xr}Mg_{xr}O$ ADQWs with $L_{b1} = 4$ nm, $L_{w1} = 5$ nm, $L_{b2} = 7$ nm, $L_{w2} = 3$ nm, $xc = 0.4$, and $xr = 0.4$, for the transition from (a) E_1 to E_2, (b) E_2 to E_3, and (c) E_1 to E_3.

Figure 9 shows the xl-dependent OACs for ADQW1 and ADQW2. It can be seen from Fig. 9(a), the distance between the peaks of ADQW1 and ADQW2 becomes bigger as xl increases. For ADQW2, the BEFs in the left barrier is strengthened gradually as increase of xl that is equivalent to narrowing L_{b1} to enlarge the electron energy level intervals. Consequently, the exciton energy level intervals become larger to shift the OACs toward a smaller λ. Contrary to this phenomenon, the BEFs in the left barrier in ADQW1 are opposite to that in ADQW2, a red shift occurs in the former. In Fig. 9(b), the differences of average positions between electrons and holes increase speedily due to the strengthened BEFs in both wells, the Coulomb interaction are weaken and the intervals of excitonic energy levels decrease for ADQW2. Whereas the BEFs in both wells are weakened as increase of xl for ADQW1. Thus the OACs have a red shift and a blue one for ADQW2 and ADQW1, respectively. The peaks merge together at $xl = 0.48$. For the transition from E_1 to E_3 mainly comes from the contribution of the hole distributed in the right well, and the variation of xl has a slight influence on the hole to bring an unobvious change on the OACs for the two kinds of ADQWs in Fig. 9(c).

4. Conclusions

Our computed results for OACs for exciton interstate transition show the following conclusions. The BEFs in ADQWs tilt the conduction and valance bands to influence the exciton energy levels and exciton types. Firstly, the exciton types occur a transformation when an electron at state e_2 participates a transition in ADQW2 for $L_{w1} = L_{w2}$ to mutate OACs. Secondly, the electron-involved exciton transitions are more sensitive to the change of size and composition than that of hole-involved for ADQW2 and ADQW1. Finally, the peaks of OACs in the two kinds of QWs merge together under some special conditions and this is helpful to both of theory and experiment.

References

[1] Sato S and Satoh S 1999 *Elctron. Lett.* **35** 1251
[2] Salhi A, Rouillard Y, Angellier J, Grech P and Vicet A 2004 *Elctron. Lett.* **40** 424
[3] Simoyama T, Yoshida H, Kasai J I, Mozume T and Ishikawa H 2003 *IEEE Photon. Tech. Lett.* **15** 1363
[4] Choy W C H, Li E and Weiss B 1998 *IEEE J. Quantum Electron.* **34** 1846
[5] Zhang Y J, Zhang X H, Tang B, Tian C, Xu C Y, Dong H X and Zhou W H 2018 *Nanoscale* **10** 14082
[6] Zhang X H, Zhang Y J, Dong H X, Tang B, Li D H, Tian C, Xu C Y and Zhou W H 2019 *Nanoscale* **11** 4496
[7] Ju Z G, Shan C X, Yang C L, Zhang J Y, Yao B, Zhao D X, Shen D Z and Fan X W 2009 *Appl. Phys. Lett.* **94** 101902
[8] Park S-H and Ahn D 2005 *Appl. Phys. Lett.* **87** 253509
[9] Yano M, Hashimoto K, Fujimoto K, Koike K, Sasa S, Inoue M, Uetsuji Y, Ohnishi Y T and Inaba K 2007 *J. Cryst. Growth* **301–302** 353
[10] Takeuchi I, Yang W, Chang K S, Aronova M A, Venkatesan T, Vispute R D, and Bendersky L A 2004 *J. Appl. Phys.* **94** 7336
[11] Fan X F, Sun H D, Shen Z X, Kuo J L and Lu Y M 2008 *J. Phys: Condens. Matter* **20** 235221
[12] Riane H, Mokaddem A, Temimi L, Doumi B, Bahlouli S and Hamdache F 2017 *J. Adv. Manuf. Tech.* **89** 629
[13] Djelal A, Chaibi K, Tari N, Zitouni K and Kadri A 2017 *Superlattice Microst.* **109** 81
[14] Zippel J, Heitsch S, Stölzel M, Müller A, Wenckstern H, Benndorf G, Lorenz M, Hochmuth H and Grundmann M 2010 *J. Lumin.* **130** 520
[15] Segawa Y, Sun H D, Makino T, Kawasaki M and Koinuma H 2015 *Phys. Status Solidi A* **192** 14
[16] Stachowicz M, Pietrzyk M A, Sajkowski J M, Przezdziecka E, Teisseyre H, Witkowski B, Alves E and Kozanecki A 2017 *J. Lumin.* **186** 262
[17] Yu F M, Zhang L and Guo K 2011 *Superlattice Microst.* **50** 128
[18] Gu Z, Zhu Z N, Wang M M, Wang Y Q, Wang M S, Qu Y and Ban S L 2017 *Superlattice Microst.* **102** 391
[19] Song L Y, Han Z Q, Zan Y H and Ban S L 2019 *Opt. Commun.* **444** 142
[20] Asgari A, Safa S and Mouchliadis L 2011 *Superlattice Microst.* **49** 487
[21] Grigoryev P S, Kurdyubov A S, Kuznetsova M S, Ignatiev I V, Efimov Y P, Eliseev S A, Petrov V V, Lovtcius V A and Shapochkin P Y 2016 *Superlattice Microst.* **97** 452
[22] Tan C M, Xu J M and Zukotynski S 1993 *J. Appl. Phys.* **73** 2921
[23] Brounkov P, Benyattou N T and Guillot G 1996 *J. Appl. Phys.* **80** 864
[24] Meng L, Zhang J, Li Q and Hou X 2015 *J. Nanomater.* **2015** 7
[25] Xia C, Zhang H, An J, Wei S and Jia Y 2014 *Phys. Lett. A* **378** 2251
[26] Senger R T and Bajaj K K 2003 *Phys. Rev. B* **68** 205314
[27] Elangovan P, John Peter A and Kyoo Yoo C 2013 *J. Lumin.* **143** 314
[28] Shi J J and Goldys E M 1999 *IEEE T. Electron. Dev.* **46** 83
[29] Miranda G L, Mora-Ramos M E and Duque C A 2013 *Physica B: Condens. Matter* **409** 78
[30] Gopal P and Spaldin N A 2006 *J. Electron. Mater.* **35** 538
[31] Duan Y, Qin L, Tang G and Shi L 2008 *Eur. Phys. J. B* **66** 201
[32] Furno E, Chiaria S, Penna M, Bellotti E and Goano M 2010 *J. Electron. Mater.* **39** 936
[33] Tanaka H, Fujita S and Fujita S 2005 *Appl. Phys. Lett.* **86** 192911
[34] Djelal A, Chaibi K, Tari N, Zitouni K and Kadri A 2017 *Superlattice Microst.* **109** 81
[35] Xu Y N and Ching W Y 1991 *Phys. Rev. B* **43** 4461
[36] Park S H and Ahn D 2007 *Opt. Quantum Electron.* **38** 935
[37] Coli G and Bajaj K K 2001 *Appl. Phys. Lett.* **78** 2861
[38] Su S C, Zhu H, Zhang L X, He M L, Zhao Z, Yu S F, Wang J N and Ling F C C 2013 *Appl. Phys. Lett.* **103** 131104